MAC/GMC Code Enhanced for Coupled Electromagnetothermoelastic Analysis of Smart Composites

Intelligent materials are those that exhibit coupling between their electromagnetic response and their thermomechanical response. This coupling allows smart materials to react mechanically (e.g., an induced displacement) to applied electrical or magnetic fields (for instance). These materials find many important applications in sensors, actuators, and transducers.

Recently interest has arisen in the development of smart composites that are formed via the combination of two or more phases, one or more of which is a smart material. To design with and utilize smart composites, designers need theories that predict the coupled smart behavior of these materials from the electromagnetothermoelastic properties of the individual phases. The micromechanics model known as the generalized method of cells (GMC) has recently been extended to provide this important capability (ref. 1). This coupled electromagnetothermoelastic theory has recently been incorporated within NASA Glenn Research Center's Micromechanics Analysis Code with Generalized Method of Cells (MAC/GMC) (ref.2). This software package is user friendly and has many additional features that render it useful as a design and analysis tool for composite materials in general, and with its new capabilities, for smart composites as well.

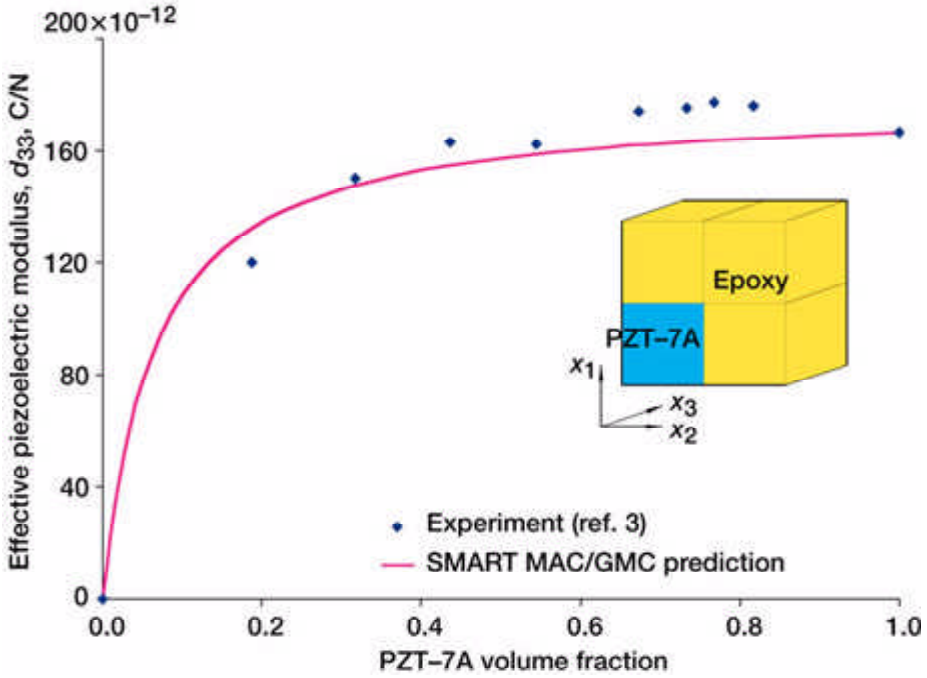

MAC/GMC prediction compared with experimental results for the "effective piezoelectric modulus" $d^*_{33} = e^*_{3k} S^*_{k3}$, where S_{ij} are the effective compliance components, of a continuous-fiber PZT-7A/epoxy composite.

Long description Plot comparing Smart MAC/GMC predictions with experimental data (from ref. 3) for the effective piezoelectric modulus (d_{33}) of the PZT-7A/epoxy smart composite. The

horizontal axis represents the composite's fiber volume fraction, spanning from zero to one. The vertical axis represents the effective piezoelectric modulus and spans from zero to 200 in units of 10^{-12} C/N. The curve representing the Smart MAC/GMC prediction starts at zero effective piezoelectric modulus, zero fiber volume fraction and then rises rapidly over the first 0.2 fiber volume fraction to approximately $130\times^{-12}$ C/N. The curve then levels off, reaching a maximum of $165\times^{-12}$ C/N at a fiber volume fraction of one. The 10 plotted experimental data points match up reasonably well with the Smart MAC/GMC prediction. The prediction is essentially right on (considering scatter) at the lower fiber volume fractions (below 0.6), but is slightly lower than the experiment in the 0.7 to 0.9 fiber volume fraction range.

The results shown here were generated to demonstrate and validate the capabilities of the enhanced MAC/GMC code. The preceding figure compares MAC/GMC predictions with experimental results (ref.3) for a PZT-7A/epoxy composite. The simple 2-by-2 GMC repeating unit cell depicted in the figure was employed for the analysis. Clearly, the agreement is good, indicating MAC/GMC's ability to predict the effective piezoelectric properties of smart composites. The next figure highlights MAC/GMC's simulated loading capabilities along with its ability to examine more refined unit cell geometries. The simulated loading is in the form of an applied electric field component, $E3$, while all other quantities besides $D3$ are held fixed at zero. Results show the amount of mechanical strain that is induced as the electric field is applied. Because of the refined unit cell geometry employed in the simulation, and the fact that the GMC theory provides predictions for the microscale fields within composite materials, the local fields shown in the final figure can be generated. The contour plots shown represent the internal fields that arise at the end of the simulation, when the applied electric field, $E3$, reaches 2.0 MV/N. It is important to note that although all global stress components on the composite are zero, MAC/GMC clearly shows that significant stresses arise internally in response to the applied electric field. This microscale capability inherent to GMC also allows the incorporation of submodels within MAC/GMC to represent local phenomena such as damage, interfacial debonding, and viscoplasticity.

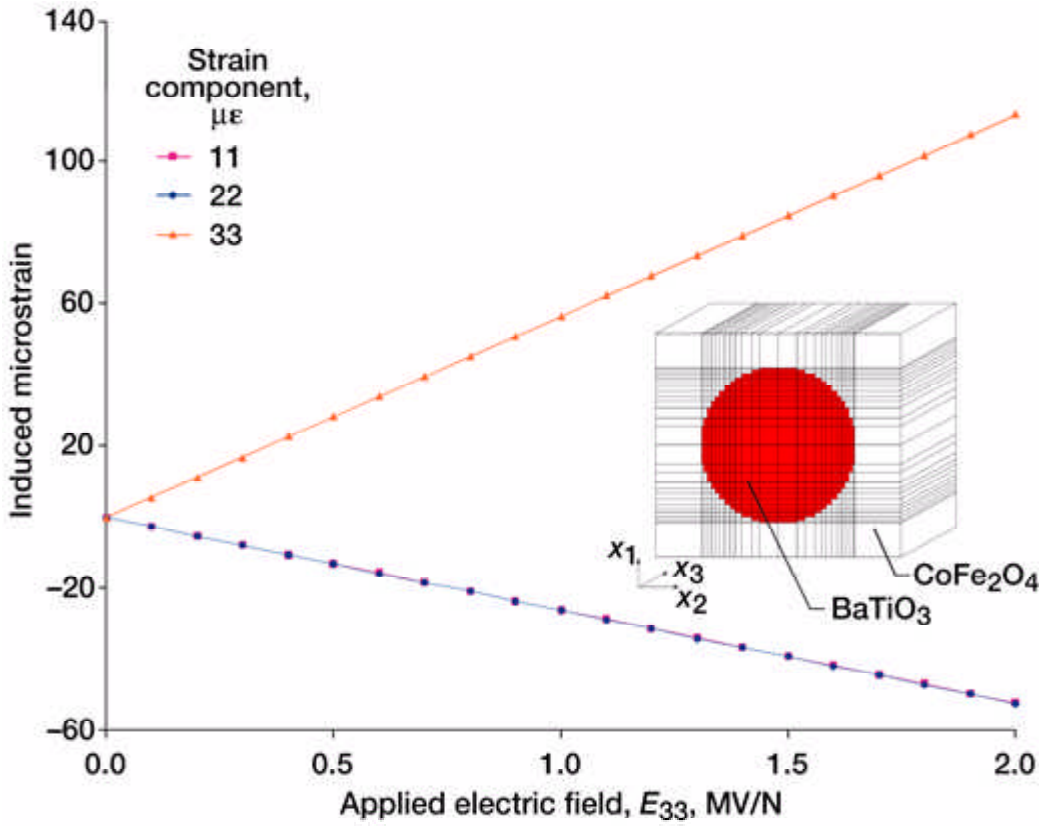

MAC/GMC prediction for the mechanical response of 35-vol% continuous-fiber $BaTiO_3/CoFe_2O_4$ to the applied electric field loading, E_{33}.

Long description Plot representing predictions for a 35% BaTiO3/CoFe2O4 smart composite that has been simulated using a refined 26 by 26 subcell GMC repeating unit cell. This rectangular unit cell (which is composed of rectangular subcells) is also shown in the figure, and the well-represented circular fiber cross section is evident. The unit cell shows that the continuous-fiber direction coincides with the x_3-direction, whereas the x_1- and x_2-directions are transverse to the fiber. The plot's horizontal axis represents the simulated electric field (E_{33}) applied to the smart composite and spans from 0 to 2 MV/N. The vertical axis represents the global microstrain induced in the composite as a result of the applied electric field and spans from -60 to 120. The plot contains three simulated curves, one for each of the three normal strain components. All three curves start at zero induced microstrain for zero applied electric field, and all three curves are linear. The 33-microstrain component curve rises from 0 to 113 at E_{33} = 2.0 MV/N, whereas the 11- and 22-microstrain component curves are nearly coincident, falling from 0 to -52 at E_{33} = 2.0 MV/N. Thus, the figure shows that, in response to the simulated applied electric field, Smart MAC/GMC predicts that the composite expands in the fiber direction and contracts in the two transverse directions.

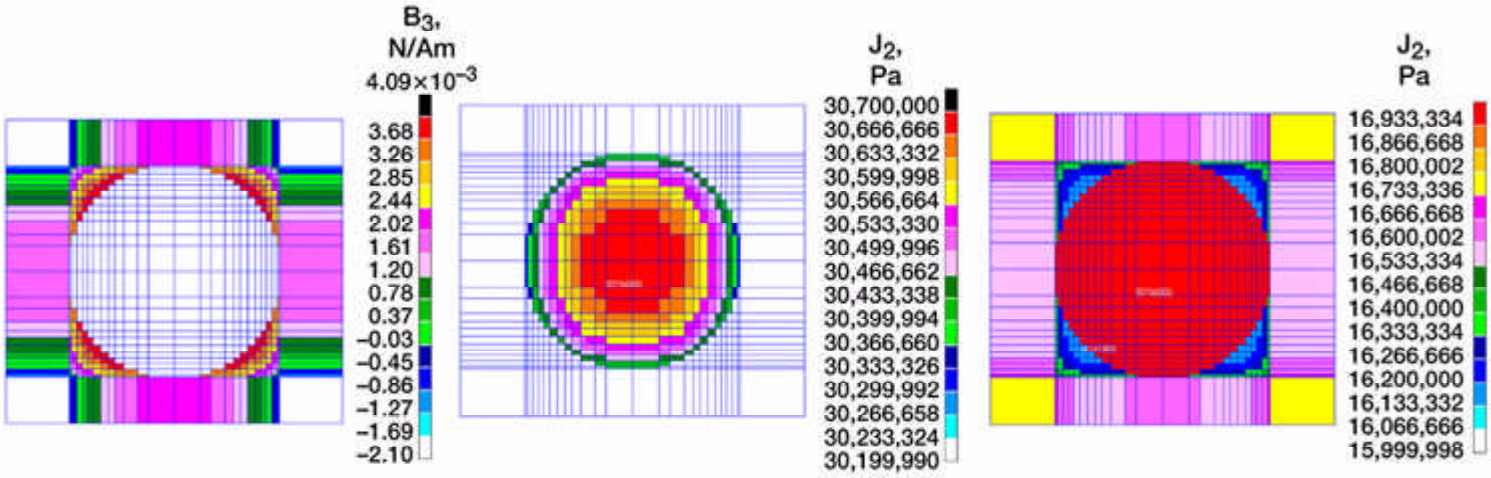

MAC/GMC prediction for the internal microfields within 35-vol% continuous-fiber $BaTiO_3/CoFe_2O_4$ at an applied electric field load level of E_{33} = 2.0 MV/m. B_3 = magnetic flux, J_2 = sqrt[(3/2)($S_{ij}S_{ij}$)], where S_{ij} = stress deviator components.

Long description Three contour plots of the microfields within the 35% $BaTiO_3/CoFe_2O_4$ smart composite whose global behavior was plotted in the preceding figure. All three contour plots are representative of the end of the simulated applied loading, when the applied electric field attains its maximum magnitude of 2 MV/N. The first contour plot represents the induced magnetic flux in the composite, B_3, in units of N/Am. The magnetic flux throughout the $BaTiO_3$ fiber is negative, in the range of -2.10×$^{-3}$ to -1.69×-3 N/Am. The magnetic flux in the $CoFe_2O_4$ matrix, on the other hand, spans the full range of the plot's scale, from -2.10×-3 to 4.09×-3 N/Am. The magnetic flux in the matrix exhibits a high degree of symmetry and attains its maximum magnitude in the region directly adjacent to the fiber. The two additional contour plots represent the J_2 stress invariant in the smart composite. One plot highlights the J_2 field in the fiber, whereas the other highlights the J_2 field in the matrix. The overall magnitudes of the J_2 field in each phase of the composite are sufficiently dissimilar so as to necessitate employing two separate plots. The plot highlighting the $BaTiO_3$ fiber indicates that the J_2 field attains a maximum value of 30.7 MPa near the center of the fiber. The J_2 field decreases radially out from the center of the fiber to a minimum of approximately 30.3 MPa. The magnitude of the J_2 field is lower in the $CoFe_2O_4$ matrix, ranging from approximately 16.9 MPa in the corners of the repeating unit cell (that are farthest from the fiber) to 16.1 MPa in the regions directly adjacent to the fiber.

References

1. Aboudi, Jacob: Micromechanical Prediction of the Effective Behavior of Fully Coupled Electro-Magneto-Thermo-Elastic Multiphase Composites. NASA/CR-2000-209787, 2000.

2. Arnold, S.M., et al.: Micromechanics Analysis Code With Generalized Method of Cells (MAC/GMC): User Guide. Version 3, NASA/TM-1999-209070, 1999.

3. Chan, H.L.W.; and Unsworth, J.: Simple-Model for Piezoelectric Ceramic Polymer 1-3 Composites Used in Ultrasonic Transducer Applications. IEEE Trans. Ultrason. Ferroelectr. Freq. Control, vol. 36, no.4, 1989, pp. 434-441.

Glenn contact: Dr. Steven M. Arnold, 216-433-3334, Steven.M.Arnold@grc.nasa.gov
Authors: Dr. Brett A. Bednarcyk, Dr. Steven M. Arnold, and Prof. Jacob Aboudi

Headquarters program office: OAT

Programs/Projects: RAC